SECED 2023 Conference
Earthquake Engineering & Dynamics for a Sustainable Future
14-15 September 2023, Cambridge, UK

CODE-BASED SEISMIC PERFORMANCE ASSESSMENT OF HIGH-RISE TUNNEL-FORM BUILDINGS IN TURKEY

Sahin DEDE[1], Tiziana ROSSETTO[2], Ufuk HANCILAR[3], Fabio FREDDI[4]

Abstract: *Tunnel-form buildings are one of Turkey's most common typologies for mass housing projects. They are known for their rapid construction process, relatively lower construction costs and shorter construction time. These structures are mainly composed of lightly reinforced thin-sectioned shear walls, coupling beams and slabs and can reach up to 20 stories or even more in some cases. The design of these structures is typically based on force-based linear elastic procedures and relies on the behaviour factor and dominant vibration modes to estimate earthquake forces. Shear walls are designed and detailed according to frame and dual systems regulations. Moreover, the minimum reinforcements required by the code are usually sufficient since the shear wall area to floor area is high. In previous earthquakes, low- and mid-rise tunnel-form buildings designed according to current standards exhibited high seismic performance. However, some drawbacks and limitations may characterise the design of taller structures. In this context, the present paper investigates the seismic performance of a 14-storey case study residential tunnel-form building located in Istanbul and considers two editions of the Turkish Building Seismic Code (i.e., the TBSC 2007 and 2018) for the performance assessment. A detailed non-linear finite element (FE) model was developed in OpenSeesPY to perform non-linear time-history analyses considering a set of natural ground motion records. The numerical model considers the inelastic behaviour of the shear walls through fibre-based distributed plasticity elements aggregated with the bilinear shear response. The elastic response of the FE model was validated against the experimental results from ambient vibration monitoring. The comparative seismic performance assessment shows that the TBSC 2018 results in more severe damage estimation, hence highlighting potential drawbacks of buildings designed with previous standards.*

Introduction

Tunnel-form is a formwork system that allows for casting walls and slabs in one operation, resulting in a cellular reinforced concrete (RC) structure. The tunnel formwork is typically made up of a series of interlocking steel panels that are assembled together to create a complete formwork structure. Once the formwork is in place, concrete is poured into the cavity, which creates the walls and floors of the building in a single continuous pour. After curing, the formworks are removed from each cell and installed on the upper storey. The system creates a concrete shear walls load-bearing structure that can be used in a wide variety of applications. It is most suitable for mass housing and fast-build projects that require more repetitions at a faster rate of building construction. While the initial cost of formwork is high, it is typically more than made up for by faster construction, the number of repetitions, zero rework, and low maintenance costs.

This typology has often been preferred in different countries, including those in seismic-prone regions. Tunnel-form buildings have shown good seismic performance during past seismic events, particularly for low- to mid-rise structures (Yakut and Gulkan, 2003; Balkaya and Kalkan, 2003). However, there may still be some drawbacks in the seismic performance of taller structures, as they exhibit a more complex response and rely on thin-sectioned, lightly reinforced shear walls. Existing studies have shown that high-rise tunnel-form buildings may suffer serious damage (Gallardo *et al.*, 2021; Ugalde *et al.*, 2019; Deger and Wallace, 2015).

In Turkish practice, similar to other countries, these buildings are designed following force-based linearly elastic design methods considering a behaviour factor (R). Dominant vibration modes are used to estimate statically equivalent earthquake forces, while detailings of shear walls are

[1] Research Student, University College London, London, UK, sahin.dede.21@ucl.ac.uk
[2] Professor, University College London, London, UK
[3] Dr, Bogazici University, Istanbul, Turkey
[4] Dr, University College London, London, UK

achieved following regulations given for the frame and dual systems. Moreover, owing to larger levels of total shear wall area on a floor, both editions of the Turkish Building Seismic Code (i.e., TBSC 2007 and TBSC 2018) allow a slight reduction in the thickness of shear walls in tunnel-form buildings compared to shear walls in dual systems. However, some drawbacks and limitations of tunnel-form buildings have been recently recognised, resulting in an update of the design guidelines. Furthermore, TBSC 2018 introduced significant changes in the definition of performance objectives and assessment procedures, *i.e.,* considerable differences exist between the TBSC 2007 and TBSC 2018.

The present study considers an existing 14-storey tunnel-form building in Istanbul to evaluate its seismic performance and to critically discuss the differences observed performing the assessment according to the former and current editions of the Turkish seismic codes, TBSC 2007 and TBSC 2018. The considered case study structure is representative of a large stock of tunnel-form buildings constructed in several mass housing projects in Istanbul and potentially extending to other parts of Turkey. The results allow for shedding some light on the vulnerable points of such buildings and support the development of code recommendations.

Case study structure and Finite Element (FE) modelling

Case study structure

Figure 1 shows the plan and elevation views of the existing case study tunnel-form building selected to perform the seismic performance assessment according to the two editions of the Turkish Building Seismic Code. This particular building was selected because of the possibility of performing ambient vibration measurements, which have been successively used to validate the numerical model. The case study is a 14-storey building with a constant interstory height of 2.8 m, including the basement, enclosed by continuous shear walls, giving a total height of 39.2 m. The floor layout is identical at all stories, has overall dimensions of 27.0 m × 21.6 m in plan, and results in 520 m^2 of floor area. There are 26 shear walls with 0.2 m thickness at each story, and they take up 6.44% of the total floor area. In addition to shear walls, each story has 12 columns with three different section dimensions of 0.2 m x 0.2 m, 0.2 m x 0.95 m, and 0.2 m x 1.25 m. Shear walls and columns are accompanied by 0.15 m thick slabs and 27 beams with varying depths.

The seismic design was performed according to the specifications of the TBSC 2007. Concrete with compressive strength of f_c = 30 MPa was used for all structural members. Two different steel classes were used for reinforcements, respectively, with yield strength f_y equal to 500 MPa and 420 MPa. The first category was used for shear wall web regions, while the second category was used for shear wall boundary regions, columns, beams, and slabs. The provisions of the TBSC 2007 for the high-ductility class were followed for the design of all structural members. Ground- and first-storey shear walls have reinforcement ratios ranging between 0.4%-0.7%, while shear walls in other stories have reinforcement ratios ranging between 0.3%-0.6%. Shear walls along the X-direction are coupled through conventionally reinforced squat coupling beams having a span-to-depth ratio of less than 2.

Figure 1. Case study structure: (A) plan and (B) elevation views.

Finite Element (FE) modelling

A state-of-the-art 3D finite element (FE) model of the case study building has been developed in OpenSeesPY (Zhu *et al.,* 2018). Line elements were used to represent all structural members except slabs and peripheral basement walls. Shear walls and wall-like wide columns were modelled adopting the wide-column analogy where section centroids are connected to surrounding nodes by rigid beams. Shear walls, columns, and beams were modelled by a fibre-based distributed plasticity approach using '*nonlinearBeamColumn*' elements with '*Concrete01*' and '*Steel02*' material models to represent confined concrete, unconfined concrete and steel reinforcements. Mander *et al.* (1988) model was used to estimate the properties of the confined concrete within the shear wall boundaries, columns, and beams. Geometric nonlinearities were included by '*Pdelta*' coordinate transformation command in OpenSeesPY. Damping forces other than the hysteretic damping of the materials were modelled by Rayleigh damping according to the first and second vibration modes with a damping factor equal to 5%.

Since shear walls are the primary structural member of tunnel-form buildings, their modelling has a significant impact on the global response of the numerical model. Experimental studies and post-earthquake observations (Wallace, 2012; Pugh *et al.*, 2015) have shown that shear walls, especially thin-sectioned shear walls, like those used in tunnel-form buildings, mainly suffer from concrete crushing, reinforcement buckling, and reinforcement fracture. These failure modes cannot be directly captured through fibre-based models. Hence, to capture these non-simulated failure modes, material models were modified using the '*MinMax*' command to exhibit a rapid strength loss after specific strain limits are exceeded. In this regard, the steel reinforcements' buckling strain was assumed equal to the crushing strain of surrounding concrete, corresponding to a concrete strength loss of 80%. Similarly, the steel reinforcements' fracture in tension was assumed to occur at 5% tensile strain (Pugh *et al.*, 2015; Gogus and Wallace, 2015). In addition, material regularisation was conducted, by following the recommendations of Pugh *et al.* (2015), to overcome deformation localisation in vertical members. Lastly, an uncoupled shear behaviour was aggregated on the fibre sections of shear walls, columns, and beams by using the '*section Aggregator*' command in OpenSeesPY. For each element, a bilinear shear force-shear deformation relationship was defined using '*Hysteretic*' material, where the shear modulus was reduced by 50%, according to TBSC 2018. Elastic membrane plate elements were employed for slabs and peripheral basement walls. For these elastic elements, cracked section stiffness was considered by reducing their flexural stiffness to 25% and 50%, respectively, as per TBSC 2018.

The elastic response of the FE model was validated against the experimental results from ambient vibration monitoring. For the sake of brevity, the details of the ambient vibration monitoring and the data processing are not provided here. However, the Fourier spectral analysis of these recorded low-amplitude vibrations showed that the first three fundamental periods are between 1.7 Hz-2.0 Hz. The first mode is dominated by torsion, whereas the second and third modes are dominated by a translational response approximately with the same periods. Since ambient vibration measurement provides the response under low-amplitude motions, the obtained data provide information on the elastic response. For comparison purposes, the numerical model was modified to disregard the cracked section stiffness and G_{eff} from the model. The fundamental vibration periods of the modified and the original FE models are provided in Table 1.

Mode	**Finite element model without cracked section stiffness**	**Finite element model with cracked section stiffness**
First Mode (Torsional)	0.52 s (1.92 Hz)	0.64 s (1.56 Hz)
Second Mode (Translational X)	0.50 s (2.00 Hz)	0.58 s (1.72 Hz)
Third Mode (Translational Y)	0.48 s (2.08 Hz)	0.55 s (1.82 Hz)

Table 1. Fundamental periods of the case study structure.

Seismic performance assessment: TBSC 2007 and TBSC 2018

Although TBSC 2007 and 2018 differ remarkably in terms of limit states' definition and seismic hazard, the recommended seismic performance assessment methods for buildings' structures are similar. Both codes suggest linear and non-linear static and dynamic assessment procedures with restrictions in their application based on several criteria, such as total height and irregular

behaviour. In contrast to linear analysis and non-linear static analysis methods, non-linear time history analysis can be applied to all types of buildings. Being the case study dominated by a torsional mode of vibration, the performance assessment required performing non-linear time history analyses.

The present work assumes full knowledge of the structure. Hence, the FE model was generated with a confidence factor equal to 1 for both the TBSC 2007 and 2018. This corresponds to the assumption that the as-built state of the building fully complies with the design (*e.g.,* no reduction of the material properties, no amplified loads). Nodal masses were calculated as compatible with the design load according to the following formulation (*1*):

$$G + Q_e \tag{1}$$

where G is the dead load and Q_e is the live load effect corresponding to 30% of total live loads. The masses were distributed among the joints at each story level based on the dead loads, live loads, and self-weight of the system. So far, all provided information includes common aspects of both codes. The following sections present the steps where the two codes differ from each other.

Gravity analysis

The TBSC 2007 and 2018 diverge in the definition of load combinations for gravity analysis which correspond, respectively, in the following Eq.s 2 and 3:

$$G + Q_e + E_d^{(H)} \tag{2}$$

$$G + Q_e + 0.2S + E_d^{(H)} + 0.3E_d^{(Z)} \tag{3}$$

where $E_d^{(H)}$ is horizontal earthquake loads, and S is snow load. To facilitate the comparison, the snow load is disregarded in the present study. Therefore, the only difference between the gravity loads applied is the statically applied vertical earthquake load, $E_d^{(Z)}$, defined as follows (*4*):

$$E_d^{(Z)} = (2/3)S_{DS}G \tag{4}$$

where S_{DS} is the short period design spectral acceleration coefficient obtained for DD-2 level ground motion. For the considered case study building, this additional vertical load defined in the TBSC 2018 corresponded to an increase of 18.2% to the total gravity action of the TBSC 2007.

Ground motion selection and non-linear time history analysis

The NGA-West2 (Ancheta *et al.*, 2014) database was used to define a suitable set of records for the non-linear time history analyses. The minimum number of ground motions required is different in the two codes, *i.e.,* 7 and 11 pairs of records for the TBSC 2007 and 2018, respectively. This work used the same set of 11 pairs of records to facilitate the comparison of the results between the two codes. The magnitude (M_w) used for the ground motion selection ranges between 6.5 and 7.5. This range was selected based on the estimated magnitude levels for the expected Marmara Sea earthquake and relevant scenario earthquakes in the literature (Erdik *et al.*, 2003; Cakti *et al.*, 2019). Considering the spatial distribution of tunnel-form buildings in Istanbul, the distance to the fault line (R_{jb}) was taken between 20 and 75 km. All records were selected from strike-slip events to represent the fault mechanism of the relevant segment of the North Anatolian Fault (NAF). A maximum of 3 records from the same event were used to prevent the dominance in the ground motion pool. The case study building is located on a ZC soil type according to TBSC 2007, *i.e.,* $V_{s,30}$ ranging between 300-700 m/s. Therefore, stations from similar values were preferred. The selected records were scaled to match the DD-2 level design spectra with a return period T_R = 475 years. All scaling factors (SFs) ranged between 1.5 and 3.0.

Table 2 summarises the selected records and the relevant parameters. SFs were defined such that the records comply with the requirements of both codes, and Figure 2 shows the calculated average spectra against the different DD-2 level design spectra. The TBSC 2018 states that the resultant horizontal spectrum of selected ground motions shall be obtained by taking the square root of the sum of the squares (SRSS) of the two horizontal components of each earthquake record set. These resultant spectra must be scaled such that their average amplitude is higher than 1.3 times the DD-2 design spectra of TBSC 2018 for periods between $0.2T_p$-$1.5T_p$, where T_p is the fundamental vibration period of the structure. On the other hand, TBSC 2007 states that the resultant spectra must be scaled such that their average amplitude is higher than 0.9 times

the DD-2 design spectra of TBSC 2007 in the range of periods between the $0.2T_1$-$2.0T_1$, where T_1 is the first natural vibration period of the building along the earthquake direction.

The selected and scaled ground motions were applied to the system following gravity analysis. Each set was applied twice to the system by changing the angle of application from 0 degrees to 90 degrees, resulting in 22 (11×2) non-linear time history analyses for each code.

Record Sequence Number	Earthquake Name	Year	Station Name	Magnitude	R_{jb} (km)	V_{s30} (m/sec)	Scaling Factor
902	Big Bear	1992	Desert Hot Springs	6.46	39.52	359.00	2.077
1118	Kobe	1995	Tadoka	6.90	31.69	312.00	1.966
1160	Kocaeli	1999	Fatih	7.51	53.34	386.75	2.440
1762	Hector Mine	1999	Amboy	7.13	41.81	382.93	2.460
1794	Hector Mine	1999	Joshua Tree	7.13	31.06	379.32	2.620
3753	Landers	1992	Fun Valley	7.28	25.02	388.63	1.778
3756	Landers	1992	Morongo Valley Hall	7.28	40.67	368.20	2.328
6059	Big Bear	1992	Morongo Valley Fire S.	6.46	27.96	396.41	2.777
6060	Big Bear	1992	North Palm Springs	6.46	40.87	367.84	2.966
6971	Darfield	2010	SPFS	7.00	29.86	389.54	2.199
6980	Darfield	2010	WAKC	7.00	72.50	484.49	2.821

Table 2. Selected ground motion records and considered parameters.

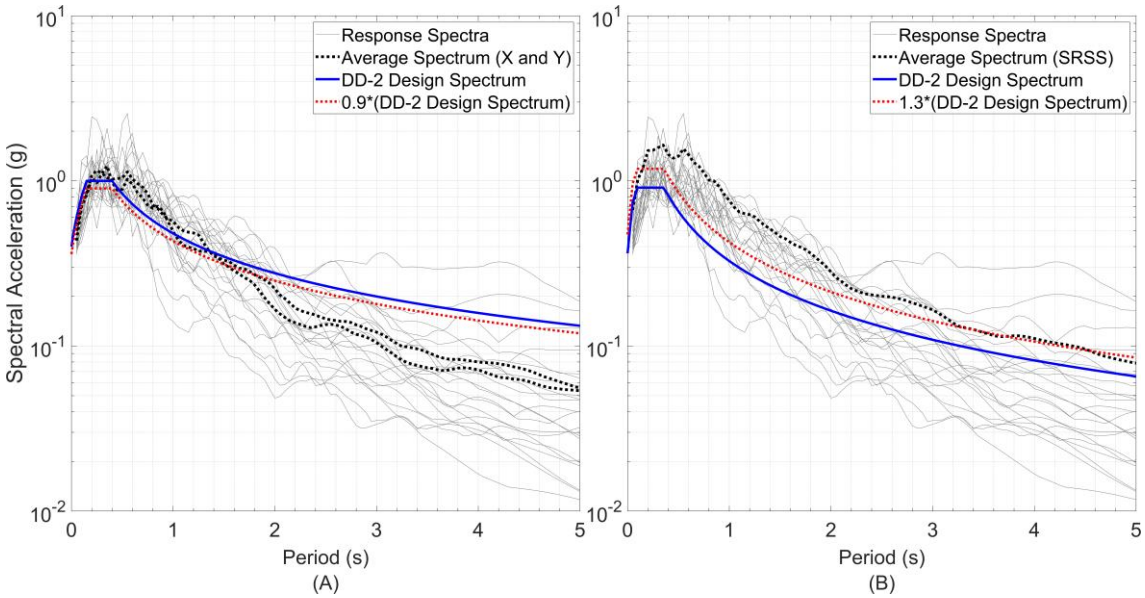

Figure 2. Ground motion spectra for (A) TBSC 2007 and (B) TBSC 2018.

Performance levels

TBSC 2007 and 2018 have four different performance levels for buildings, and each performance level has quantified definitions based on the number of damaged structural elements. Those performance levels are namely *immediate occupancy*, *life safety*, *collapse prevention* and *collapse*. Table 3 provides a quantitative description of these performance levels and relates these with the percentage of horizontal and vertical components within a specified damage state region (*i.e.,* limited damage, visible damage or extensive damage region). Only the specifications relevant to the considered case study structure are provided, while for a comprehensive discussion, the reader can directly refer to the codes. Table 3 shows that, for the same performance level, the TBSC 2018 accepts a larger number of elements within a more severe damage state region compared to TBSC 2007. However, at the same time, the TBSC 2018 provides more severe criteria for the definition of these damage states regions, as discussed in the following section.

Damage states regions

Four different damage regions are defined for ductile elements, *i.e., limited damage region, visible damage region, extensive damage region,* and *collapse*. The upper limits of these regions are

defined as damage limit states (LSs) and are described in Table 4. The seismic demand values recorded from the analyses for each component at different sections are compared with the corresponding LSs given in the codes. The *limited damage* LS refers to a limited amount of inelastic demand at the section. The *visible damage* LS refers to an amount of inelastic demand at the section that can be sustained safely without considerable loss of strength. Lastly, the *extensive damage* LS refers to a significant level of damage close to the section failure. Elements with demand values higher than these are considered in the collapse damage state region.

Seismic Code	Performance Level	Criteria for Beams	Criteria for Vertical Members
TBSC 2007	Immediate Occupancy	Up to 10% is allowed to be in visible damage region.	- Members are in the limited damage region.
	Life Safety	Up to 30% is allowed to be in extensive damage region.	- Members in extensive damage shall not bear more than 20% of the storey shear. - All other members are in the limited damage or visible damage region. - Members that surpassed limited damage at both ends shall not bear more than 30% of the storey shear.
	Collapse Prevention	Up to 20% is allowed to be in collapse region.	- Members are in the limited damage, visible damage or extensive damage region. - Members that surpassed limited damage at both ends shall not bear more than 30% of the storey shear.
	Collapse	When the above criteria are not met.	
TBSC 2018	Immediate Occupancy	- Up to 20% is allowed to be in visible damage region.	- Members are in the limited damage region.
	Life Safety	Up to 35% is allowed to be in extensive damage region.	- Members in extensive damage shall not bear more than 20% of the storey shear. - All other members are in the limited damage or visible damage region. - Members that surpassed visible damage at both ends shall not bear more than 30% of the storey shear.
	Collapse Prevention	Up to 20% is allowed to be in collapse region.	- Members are in the limited damage, visible damage or extensive damage region. - Members that surpassed visible damage at both ends shall not bear more than 30% of the storey shear.
	Collapse	When the above criteria are not met.	

Table 3. Performance level definitions.

Damage Limit States	TBSC 2007	TBSC 2018
Extensive Damage	$\varepsilon_c = 0.004 + 0.014(\rho_s/\rho_{sm}) \leq 0.018$ $\varepsilon_s = 0.06$	$\varepsilon_c = 0.0035 + 0.04\sqrt{\omega_{we}} \leq 0.018$ $\varepsilon_s = 0.4\varepsilon_{su}(0.32)$ $\theta_p = \theta_p^{(ED)}$
Visible Damage	$\varepsilon_c = 0.0035 + 0.01(\rho_s/\rho_{sm}) \leq 0.0135$ $\varepsilon_s = 0.04$	$\varepsilon_c = 0.75\varepsilon_c^{(ED)}$ $\varepsilon_s = 0.75\varepsilon_s^{(ED)}$ $\theta_p = 0.75\theta_p^{(ED)}$
Limited Damage	$\varepsilon_{cu} = 0.0035$ $\varepsilon_s = 0.01$	$\varepsilon_c = 0.0025$ $\varepsilon_s = 0.0075$ $\theta_p = 0$

Table 4. Damage limit state definitions.

TBSC 2007 defines the damage LSs of the ductile elements based on concrete strain, ε_c, and steel strain, ε_s, as reported in Table 4. In TBSC 2007, compliance is checked by comparing curvature demands to the curvature limits calculated based on the provided strain limits in Table 4. Curvature demands on elements are calculated by dividing the rotation demands by the plastic hinge length, which according to TBSC 2007, is taken as half of the section depth.

On the other side, in addition to concrete strain, ε_c, and steel strain, ε_s, TBSC 2018 defines the damage LSs also based on plastic chord rotations, θ_p. While the strain values can be directly obtained from the model, the plastic chord rotation, θ_p, can be calculated by subtracting the yield chord rotation, θ_y, from the total chord rotation demand. The yield chord rotation, θ_y, can be derived as follows *(5)*:

$$\theta_y = \frac{\phi_y L_s}{3} + 0.0015\eta\left(1 + 1.5\frac{h}{L_s}\right) + \frac{\phi_y d_b f_y}{8\sqrt{f_c}} \quad (5)$$

The readers may refer to the work of Biskinis and Fardis (2010) for further information on the parameters of this equation. The plastic chord rotation limit for the extensive damage LS, $\theta_p^{(ED)}$, is calculated as follows (*6*):

$$\theta_p^{(ED)} = \frac{2}{3}\left[(\phi_u - \phi_y)L_p\left(1 - 0.5\frac{L_p}{L_s}\right) + 4.5\phi_u d_b\right] \quad (6)$$

where ϕ_u is ultimate curvature, L_p is the length of the plastic deformation region defined as half of the section depth, L_s is shear span, and d_b is the diameter of longitudinal reinforcement.

Herein, beams were assessed through curvatures and chord rotations for TBSC 2007 and TBSC 2018, respectively. Conversely, the damage state of shear walls and wall-like wide columns were evaluated through the strain limits given in Table 4. TBSC 2018 presents considerably lower reinforcing steel strains for each LS compared to TBSC 2007. In the case of TBSC 2007, the ratio between the volumetric ratio of existing transverse reinforcement in the section and volumetric ratio of required transverse reinforcement in the section, ρ_s/ρ_{sm}, is the determining factor of confined concrete strains of LSs and it is taken as unity herein. On the other hand, concrete strain limits as per TBSC 2018 are calculated based on the mechanical reinforcement ratio of effective transverse reinforcement, ω_{we}, which is obtained through (*7*):

$$\omega_{we} = \alpha_{se}\rho_{sh,min}\frac{f_{yw}}{f_c} \quad ; \quad \alpha_{se} = \left(1 - \frac{\sum a_i^2}{6b_0h_0}\right)\left(1 - \frac{s}{2b_0}\right)\left(1 - \frac{s}{2h_0}\right) \quad (7)$$

where $\rho_{sh,min}$ is the minimum volumetric ratio of transverse reinforcement, f_{yw} is the yield strength of the transverse reinforcement, α_{se} is the efficiency coefficient of transverse reinforcement, a_i is the distance between longitudinal reinforcements surrounded by transverse reinforcement, b_0 and h_0 are the dimensions of the confined area, and s is the vertical spacing of transverse reinforcements.

Differently from TBSC 2007, the TBSC 2018 provides detailed requirements for the damage LSs definition accounting for the simultaneous effects of bending and shear force. Based on the shear force present in the component, the damage LSs are updated according to the modification factors provided in Table 5. This modification factor must be interpolated for intermediate shear demand to capacity ratios.

V_e / ($b_w d f_{ctm}$)	Modification factor
< 0.65	1.0
> 1.30	0.5

Table 5. Damage limit modification factors as per TBSC 2018.

In Table 5, V_e is the shear force present in the component, f_{ctm} is the tensile strength of the concrete, b_w and d are the section dimensions of the member. Force-controlled elements (*i.e.,* failing due to brittle mechanisms - shear failures) are considered in the collapse damage state region.

Results

A total of 22 non-linear time history analyses were conducted with the same set of ground motion records, with the same SFs and separately for the two codes (*i.e.,* the models used for the analyses differed in terms of gravity load applied). Chord rotation demands on beams and strain demands on extreme fibres of boundary and web regions of vertical members were monitored along with the shear force demands throughout all analyses. Mean values of the samples of the demand for the 22 analyses were calculated for each element of the structure and compared against the LSs definitions provided in the previous chapter.

Figure 3(a) shows the percentage of coupling beams with shear force demands greater than the capacity provided by beam transverse reinforcements. The results show that, for this particular building, the shear force capacity provided by beam transverse reinforcements was exceeded for many beams in both cases. Since both codes provide the same definition of shear force demand and capacity, only slight differences are observed due to the different gravity loads applied. Shear failure on these beams was expected due to their aspect ratio and due to the coupling with shear walls and wall-like wide columns. For such squat beams, the use of diagonal reinforcements instead of conventional detailing might increase their strength and ductility, leading to higher seismic performance. Regarding ductile failure mechanisms, as mentioned earlier, the TBSC 2018 accounts for the impact of shear force on the bending response of members through modification factors (Table 5). This results in a much higher number of beams in limited damage region in the case of TBSC 2018 when compared with the TBSC 2007 (Figure 3(b)). Apart from this, none of the cases resulted in chord rotation demands larger than limited damage.

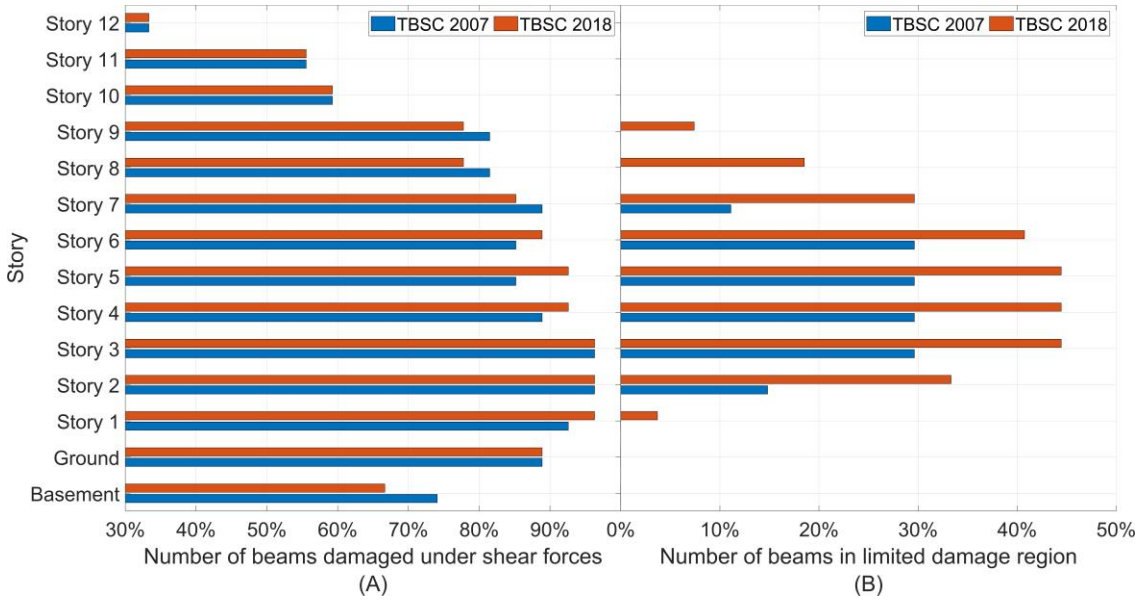

Figure 3. Number of beams with (A) damage under shear forces and (B) chord rotations.

Figure 4 shows the damage states of vertical load-bearing elements. Given damage states were obtained by comparing the strain demands on the outermost fibres of boundary regions of vertical members to the damage LSs given in Table 4.

In the case of TBSC 2007, 6 vertical members are in the visible damage region, one in the extensive damage region and one in the collapse region. These members are lying parallel to the X-direction of the building and share 46% of the total storey shear force along this direction. Members in extensive damage and collapse regions make equal contributions, corresponding to 3.5%. A more extensive damage pattern is visible in the case of TBSC 2018, where 7 vertical members are in the visible damage region, 5 in the extensive damage region and 3 in the collapse region. Differently from TBSC 2007's case, members in both directions resulted in some level of damage. These members share 51% of the total storey shear force along the X-direction and 30% of the total shear force along the Y-direction. Along the X-direction, members in the extensive damage region carry 32% of the total shear force. Overall, it can be observed that the seismic assessment performed according to the TBSC 2018 results in a remarkably more severe damage distribution of the vertical components.

The percentage of elements in a specific damage state region informs on the performance level of the structure. For beams, the results show that the shear capacity is exceeded for a large percentage of elements on all building stories. The number of beams that failed due to brittle mechanisms surpassed the criteria for collapse prevention performance level under both codes (Table 3). Conversely, for vertical elements, brittle failures were not observed, and the damage pattern is mainly dominated by flexural damage states. It can be observed that the modification factor to account for the shear force contribution in the definition of the flexural capacity suggested in the TBSC 2018 led to a much more severe damage pattern with respect to the one from the TBSC 2007. According to the TBSC 2018 assessment, the elements in the extensive damage

region carry 32% of the total story shear, exceeding the life safety performance level limit. However, despite the more severe damage scenario estimated according to the TBSC 2018, it is worth highlighting that, as reported in Table 3, none of the codes accepts any vertical element in the collapse region. In light of these results, the assessment results in the same *collapse* performance level from both codes.

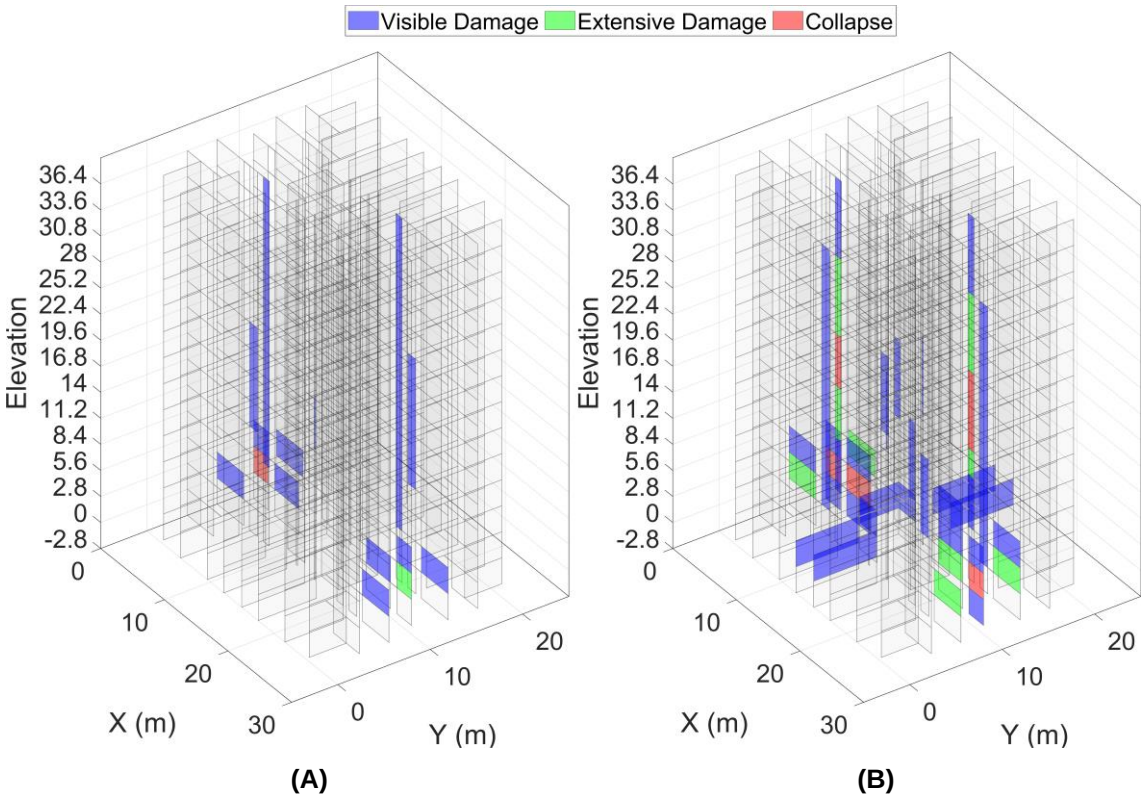

Figure 4. Shear wall damage distribution (basement walls are not shown in the figure).

Conclusion

The present study numerically investigates the seismic performance of an existing 14-storey tunnel-form building located in Istanbul following the specifications of two editions of the Turkish Building Seismic Code (*i.e.,* the TBSC 2007 and 2018). The case study represents an index project that was used to construct mass housing projects around Istanbul. This typology is distinguished by its load-bearing system in which almost all of the vertical members consisted of lightly reinforced thin-sectioned shear walls. A detailed non-linear finite element (FE) model was developed in OpenSeesPY to perform non-linear time-history analyses considering a set of natural ground motion records. The numerical model considers the inelastic behaviour of the shear walls through fibre-based distributed plasticity elements aggregated with the bilinear shear response. The elastic response of the FE model was validated against the experimental results from ambient vibration monitoring. The comparative seismic performance assessment shows that the TBSC 2018 results in more severe damage estimation for all types of structural elements, highlighting potential drawbacks of buildings designed with previous standards. Key aspects of this result include the increased gravity load and the reduced capacity in the vertical elements due to the interaction with the shear forces considered in the TBSC 2018. These results show that TBSC 2018 is more conservative than its former version. However, the seismic performance assessment show that the considered case study structure falls into the collapse performance level according to both codes, *i.e.,* the TBSC 2007 and TBSC 2018. These preliminary results highlight some drawbacks of the considered case study structure and the need for advanced study to further investigate their performance under different scenarios and propose possible solutions to increase their seismic response.

References

Yakut, A. and Gulkan, P., 2003. Housing report Tunnel form building. Earthquake Engineering Research Institute (EERI) an International Association for Earthquake Engineering (IAEE), Turkey/report, 101.

Balkaya, C. and Kalkan, E., 2003. Non-linear seismic response evaluation of tunnel form building structures. Computers & Structures, 81(3), pp.153-165.

Gallardo, J.A., de la Llera, J.C., Santa María, H. and Chacon, M.F., 2021. Damage and sensitivity analysis of a reinforced concrete wall building during the 2010, Chile earthquake. Engineering Structures, 240, p.112093.

Ugalde, D., Parra, P.F. and Lopez-Garcia, D., 2019. Assessment of the seismic capacity of tall wall buildings using non-linear finite element modeling. Bulletin of Earthquake Engineering, 17, pp.6565-6589.

Deger, Z.T. and Wallace, J.W., 2015. Collapse assessment of the Alto Rio building in the 2010 Chile earthquake. Earthquake Spectra, 31(3), pp.1397-1425.

Turkish Building Seismic Code (2007). The Ministry of Public Works and Settlement, Ankara, Turkey.

Turkish Building Seismic Code (2018). Disaster and Emergency Presidency, Ankara, Turkey.

Zhu, M., McKenna, F. and Scott, M.H., 2018. OpenSeesPy: Python library for the OpenSees finite element framework. SoftwareX, 7, pp.6-11.

Mander, J.B., Priestley, M.J. and Park, R., 1988. Theoretical stress-strain model for confined concrete. Journal of structural engineering, 114(8), pp.1804-1826.

Wallace, J.W., 2012. Behavior, design, and modeling of structural walls and coupling beams—Lessons from recent laboratory tests and earthquakes. International Journal of Concrete Structures and Materials, 6, pp.3-18.

Pugh, J.S., Lowes, L.N. and Lehman, D.E., 2015. Non-linear line-element modeling of flexural reinforced concrete walls. Engineering Structures, 104, pp.174-192.

Gogus, A. and Wallace, J.W., 2015. Seismic safety evaluation of reinforced concrete walls through FEMA P695 methodology. Journal of Structural Engineering, 141(10), p.04015002.

Ancheta, T.D., Darragh, R.B., Stewart, J.P., Seyhan, E., Silva, W.J., Chiou, B.S.J., Wooddell, K.E., Graves, R.W., Kottke, A.R., Boore, D.M. and Kishida, T., 2014. NGA-West2 database. Earthquake Spectra, 30(3), pp.989-1005.

Erdik, M., Aydinoglu, N., Fahjan, Y., Sesetyan, K., Demircioglu, M., Siyahi, B., Durukal, E., Ozbey, C., Biro, Y., Akman, H. and Yuzugullu, O., 2003. Earthquake risk assessment for Istanbul metropolitan area. Earthquake Engineering and Engineering Vibration, 2, pp.1-23.

Cakti, E., E. Safak, U. Hancilar, and K. Sesetyan., 2019. Updating probable earthquake loss estimates for Istanbul province, Technical Report prepared for Istanbul Metropolitan Municipality (In Turkish)

Biskinis, D. and Fardis, M.N., 2010. Deformations at flexural yielding of members with continuous or lap-spliced bars. Structural concrete, 11(3), pp.127-138.